CFD OPTIMIZATION OF A TRANSONIC COMPRESSOR USING MULTIOBJECTIVE GA AND METAMODELS

Lars Ellbrant*, Lars-Erik Eriksson, Hans Mårtensson*****
***,**Chalmers University of Technology, ***Volvo Aero Corporation**
***ellbrant@chalmers.se**

Keywords: *CFD, compressor, design, optimization, metamodels*

Abstract

This paper present an automatic design process where a non-deterministic, global search optimization is utilized to optimize a first stage rotor of a highly loaded transonic compressor. The first part is focused on finding the best suited metamodel that can be used to accelerate the design process. The second part presents the results of using the meta model within the design process for an industry relevant case.

Using the radial basis functions as acceleration technique for the optimization was seen to be very successful. The meta model assisted optimization reduced the total design time from approximately 2 weeks to 3.5 days given that 8 designs could run in parallel on a cluster. The 3D optimization produced a pareto front where it was possible to select blades having either high efficiency or high stability.

1 Introduction

A modern compressor design method applicable for industrial purposes requires a fast and reliable process. The requirements in terms of aerodynamics for such a design is very often high stability along the operating line together with high efficiency at a certain operating point. To include both objectives in the design chain while minimizing the total design time requires efficient optimization algorithms together with a well planned design logic. The time and computational cost starts becoming a limitation when focus is put on the actual blade geometries, that is, once the preliminary compressor layout has been set using mean line tools and through flow methods. To find the optimal blade geometries, low fidelity CFD methods such as quasi-3D analysis are typically employed first using boundary conditions based on the through flow calculations. Once a complete 3D geometry has been defined, further optimization is normally done using a detailed 3D CFD flow solver. To save time and computational resources the largest gain would be to reduce the amount of 3D CFD analysis. This can be done if a good starting point for the 3D CFD optimization can be reached by using quasi-3D analysis in an efficient way. To reduce the optimization time even further meta models can be used as a replacement for the CFD analysis.

To solve the optimization problem various methods can be employed. A rational exploration of the design space can be utilized as a support for the designer, which has been shown to be successful in both [1] and [2]. A more sophisticated approach is to use an automatic optimization process. This can be done by coupling the geometric tool, the computational grid generator and the flow solver together with an optimizer. The optimizers can be divided into deterministic and non-deterministic methods. The deterministic methods are generally more time efficient but they are likely to find a local minima. Moreover, since information about the gradient of the objective function is required they are sensitive to noise and discontinuities. When multi-objective optimization is solved by these methods the objectives must be merged into a single objective, meaning that the trade-off between the objectives must be determined before solving the optimization problem. In spite of the mentioned drawbacks, deterministic methods have been successful in many cases such as [3] and [4].

The non-deterministic method is based on random selected function evalutations thereby reducing the risk of reaching a local minima. Also it does not require the objective functions to be continous and noise free. The method is also capable of dealing directly with multi-objective optimization problems, where the trade-off between the objectives is available in terms of a pareto-front once the optimization is converged. The main drawback is that it requires much more function evaluations compared to the deterministic methods. One solution to this problem is to replace most of the CFD analysis with a meta model. Previous work using various meta-model assisted optimizations have shown to be successful for turbo-machinery flows in [5, 6, 7, 8, 9, 10, 11, 12, 13, 14]. The work in [15] gives a good overview of using meta-models for turbomachinery design. From this previous work, meta-models such as Kriging, Radial basis functions (RBF) and Neuron Network (NN) show great potential in replacing the costly CFD evaluations.

This paper presents an automatic design process where a non-deterministic, global search optimization is utilized to optimize a first stage rotor of a highly loaded transonic compressor. The first part of this work is focused on finding a meta-model that can be used to accelerate the design process. This is done by comparing different meta models on a test case where a pure CFD based pareto front is available for comparison, presented in [16]. The second part consist of applying the best suited meta model to the redesign of a transonic rotor.

2 Design process

The automatic design process without the use of meta models have been described in [16] and can be seen in Fig. 1(a). To improve its efficiency, a meta model was built into the process as shown in Fig. 1(b).

The design process consists of an inner and outer loop. It starts in the outer loop where a trainingset is initialized. The geometries are then generated by using Volbade, an inhouse developed code at Volvo Aero Corporation (VAC). The computational grids are then created and the flow solver Volsol is here used to acquire the exact

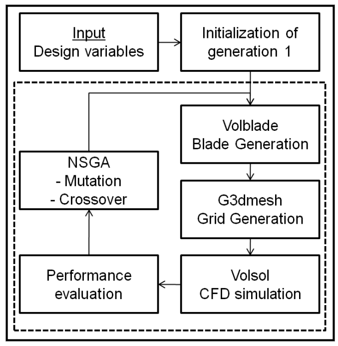

(a) Original

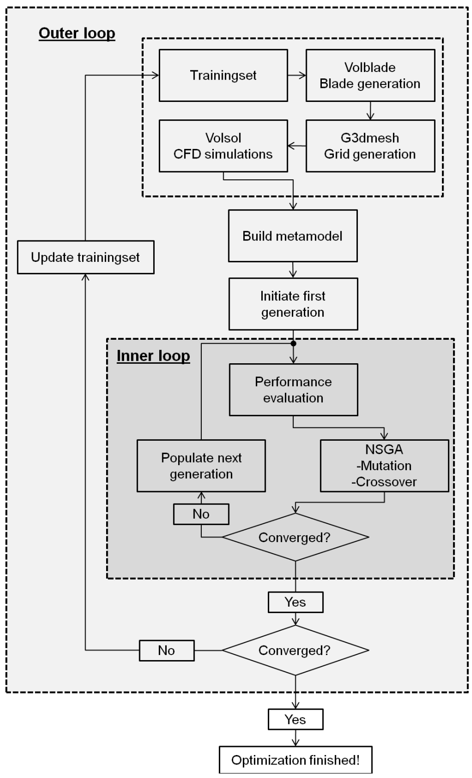

(b) Meta model assisted

Fig. 1 Design process

function values. This is the expensive part in terms of time and computational resources. Once the objectives and constraints are known the meta model is built. The process then moves to the inner loop where the global optimizer searches the design space for the optimal solutions (the pareto front). The performance evaluations are, in this loop, very fast since it only involves function evaluations on the meta model. The inner loop is converged once the location and shape of the pareto front is constant, typically after 20 generations corresponding to 30 seconds. However, the underlying data that generated the meta model is quite sparsely populated throughout the design space, thus after the first inner loop, the meta model needs to be validated. This is done by updating the trainingset with the the "virtual" pareto front from the inner loop. The flow solver is then used to evaluate the new designs in the trainingset and the "real", CFD based, pareto front can be extracted. The outer loop convergence is determined by the location and shape of the "real" pareto front.

2.1 Geometric design space

The geometric design space is constructed by using composite Non-Uniform Rational B-Splines (NURBS) [17] for each 2D blade section. This parameterization ensures a smooth blade and can generate a large number of different shapes with relatively few design variables, [17] and [18]. The underlying parameterization is defined by four NURBS curves, i.e., the leading edge, trailing edge, the pressure and suction side. A thickness distribution and a camber line defines the pressure and suction side curves while the leading and trailing edges are given by elliptical arcs. The intersection between the curves are of C1 continuity. The control points are translated as much as possible to classical compressor parameters described in more detail in [19]. The parameters describing the 2D blade section is shown in Fig. 2 and summarized in Tab. 1. The complete 3D blade is constructed from stacked 2D blades along a general stacking axis which can allow for lean and sweep. Limitations of the design variables are set so that the aero mechanical integrity and manufacture aspects are accounted for.

Table 1 Design variables

t_{le}	Leading edge thickness
t_{te}	Trailing edge thickness
s_{le}	Leading edge skewness
s_{te}	Trailing edge skewness
$t_{max,c}$	Maximum thickness over chord ratio
N	Number of blades
c_{ax}	Axial chord
inc	Incidence angle
dev	Deviation angle
ξ	Stagger angle

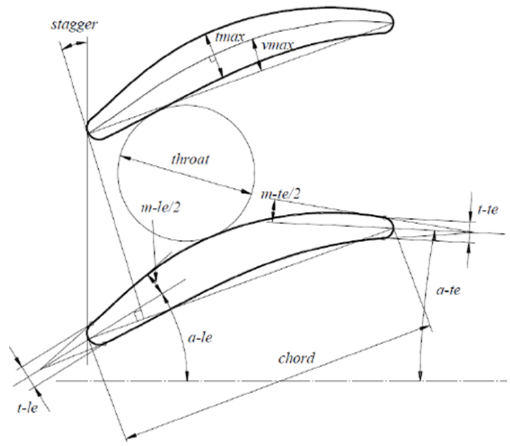

Fig. 2 Blade profile with design variables

2.2 Grid generation

The computational grid is constructed using G3dmesh, an in-house code at VAC. Using the NURBS description of the blade profile a block structured hexa-hedral grid divided into five blocks is created, see Fig. 3. Around the blade an O-grid type block is used, connected to H-type blocks.

2.3 CFD settings

To evaluate the objective functions the solver Volsol, developed by VAC, is utilized. It is a

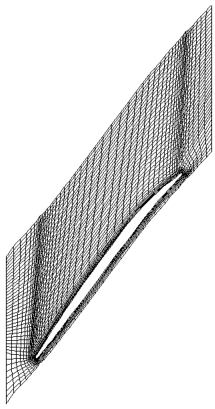

Fig. 3 Computation domain for a 2D blade section

finite volume code using a three-stage Runge-Kutta time marching method with a third order accurate upwind-biased scheme for all convective terms and a second order accurate compact centered scheme for all diffusive terms. To solve for the turbulence, the realizable k-ε turbulence model is used together with wall-functions and the Kato-Launder limiter. The blade to blade analysis referred to as the quasi-3D analysis accounts for the stream tube height variation. The code was recently validated for this type of transonic flow in [20]. Upstream of the blade row a plenum is used to represent the incoming flow from the inlet guide vane. At the inlet of the plenum, a mixed pressure boundary condition is used where P_0, T_0, β, θ , k and ε are specified. This ensures that the incoming velocity angle (in the absolute frame of reference) is fixed during the optimization. Downstream of the blade row an outlet plenum is placed where the averaged outlet static pressure is specified using an absorbing boundary condition. A mixing plane boundary type is used at the interfaces between the rotor domain and the plenums. The mixing plane formulation is based on tangential averaging and flux correction for full conservation of the fluxes. This boundary condition is an absorbing one which is necessary to avoid reflections of shocks at the interface. Detailed information about the mixing plane implementation can be found in Stridh [21]. Within the optimization two different rotational speeds are analyzed to obtain the values of the two objective functions. For each rotational speed, the compressor performance was obtained by increasing the outlet static pressure in steps.

2.4 Optimizer

The Non Sorting Genetic Algoritm (NSGA-II) is used as optimizer which is a genetic algorithm which models the evolution in nature. The first generation of designs are initialized using latin hypercube samples which gives a good spread in the design variables. The objective functions for each individual is evaluated by either the flow solver or the meta model. The evolution algorithm then forms the next generation based on non-dominated sorting amongst the individuals in such a way that the diversity among the population is maintained. The non-dominated individuals form the pareto front and the evolution is manually stopped once the pareto front is converged. Elitism is also active in order to achieve better convergence and the constraints handling is based on tournament selection. This method is implemented in modeFrontier™and is described in detail in Deb [22].

2.5 Objectives

To rate designs the maximum static pressure recovery ($C_{p,max}$) is used as a measure for stability and the pressure loss (ω) in the relative frame of reference is used to measure efficiency. Thus the optimization problem consist of the following:
Minimize: $f_1(\mathbf{x}) = \omega$
Maximize: $f_2(\mathbf{x}) = C_p$
where:

$$\omega = \frac{P_{02,isen} - P_{02}}{P_{01,rel} - P_1}$$
$$C_p = \frac{P_2 - P_1}{P_{01,rel} - P_1}$$

3 Meta models

To investigate which meta model that is suitable within an optimization of a transonic compressor blade, a test case was used. The test case consists of optimizing the rotor blade at 95% span using the full design variable set summarized in Tab. 1. The goal with the optimization was to find the pareto front describing the trade between pressure loss at design point (ω) and the maximum pressure recovery at part speed ($C_{p,max}$). The case study includes four types of meta models: least square second order polynom (2nd poly), Kriging, Neural Networks (NN) and radial basis functions (RBF).

The metamodels are rated against each other by comparing their estimate of the objective functions, denoted $\hat{f}_i(x_j)$, to the exact function, denoted $f_i(x_j)$, where x_j denotes the jth design and f_i the ith objective function. The error is measured as the averaged relative error (see Eqn. 1) and the maximum relative error (see Eqn. 2) averaged over the two objective functions.

$$E_{i,ave} = \frac{1}{d}\sum_{j=1}^{d}\left|\frac{\hat{f}_i(x_j) - f_i(x_j)}{f_i(x_j)}\right| * 100 \quad (1)$$

$$E_{i,max} = \max\left(\left|\frac{\hat{f}_i(x_j) - f_i(x_j)}{f_i(x_j)}\right| * 100\right) \quad (2)$$

The following subsections give a brief overview of each meta model, the reader is referred to the references associated with each meta model if a more detailed description is desired.

3.1 2nd order polynom

The method consists of fitting a second order polynom function to the trainingset, for more information see [23]. Since it is a regression model it will not necessarily pass directly through the known points. The equation defining a quadratic response surface is given by

$$\hat{f}(\mathbf{x}) = a_0 + \sum_{i=1}^{k} b_i x_i + \sum_{i=1}^{k}\sum_{j=1}^{k} c_{ij} x_i x_j \quad (3)$$

The coefficients are determined by least square regression analysis by fitting the model to the existing data. To solve the minimization the number of known points must be larger or equal to the amount of unknown coefficients, which can be a major drawback when the design space is high dimensional.

3.2 Kriging

Kriging is a regression model that is based on Gaussian processes originally used in geostatistics to predict gold concentration at extraction sites. The method has since then been spread to many other areas, and it has been used for turbomachinery design in [6], [7], [11] amongst others.

The mathematical model consists of two parts as shown in Eqn. 4. The first part is a polynomial function ($\hat{\beta}(\mathbf{x})$), and the second part is the realisation of a normally distributed Gaussian random process with zero mean [23].

$$\hat{f}(\mathbf{x}) = \hat{\beta}(\mathbf{x}) + Z(\mathbf{x}) \quad (4)$$

The polynomial term ($\hat{\beta}(\mathbf{x})$) constructs the global shape of the design space while $Z(\mathbf{x})$ is used to model the local behaviour by interpolation. The Gaussian correlation function, R, is used to determine how the designs influence each other as a function of their distance apart (see Eqn. 5).

$$R(x^i, x^j) = \exp\left(-\sum_{k=1}^{n} \theta_k \left|x_k^i - x_k^j\right|^{p_k}\right) \quad (5)$$

where x_k^i and x_k^j are the kth components of the sampled points and θ_k and p_k are parameters used to fit the model, [24]. The interpolant function, $Z(\mathbf{x})$, is then obtained by

$$Z(\mathbf{x}) = r^T(\mathbf{x})\mathbf{R}^{-1}(f(\mathbf{x}) - \hat{\beta}(\mathbf{x})) \quad (6)$$

where

$$\mathbf{r}^T(\mathbf{x}) = [R(\mathbf{x}, \mathbf{x}^1)R(\mathbf{x}, \mathbf{x}^2)\ldots, R(\mathbf{x}, \mathbf{x}^n)]^T \quad (7)$$

The resulting model includes not only the estimate at each point but also a complete probabilistic distribution at each point such as the error estimate. This could potentially be used to improve the model itself by iteratively using the flow solver to update the model where the error estimate is high. For more extensive theory concering construction of Kriging models, see [23], [24] and [25].

3.3 RBF

The method is an interpolator where an estimated point is a function of the euclidean distance to its neighbouring known points, see Eqn. 8. The function, ϕ, is a distribution function which are used to rank the importance of the neighbouring data. The radial function used for this study is given by Eqn. 9, where σ is a fixed scaling parameter which determines the shape of the distribution.

$$\hat{f}(\mathbf{x}) = \sum_{j=1}^{n} c_j \phi(||\mathbf{x} - x_j||/\sigma) \quad (8)$$

where:

$$\phi(r) = (1 + r^2)^{(-1/2)} \quad (9)$$

The coefficients, c_j, are obtained by requiring that the RBF model must go through the known values, see Eqn. 10, where $f(x_i)$ is the known data points. Turbomachinery design processes have been successfully accelerated using RBF, for instance in [10] and [14]. A detailed description of the underlying theory is given in [26].

$$\hat{f}(x_i) = f(x_i) \quad (10)$$

3.4 NN

Neural networks mimics the human brain, where the neurons are connected to each other as shown in Fig. 4. Following the simplified schematic in Fig. 4, the design variables are connected with each neuron in the first hidden layer, and to each connection a weight is applied. The input given to one neuron is given by Eqn. 11, where w_j are the weights, x_j the design variables and b the bias term.

$$s = \sum_{j=1}^{n} w_j x_j + b \quad (11)$$

The output of the neuron (y) is then obtained by using a transfer function, given by Eqn. 12.

$$y = \sigma(s) \quad (12)$$

The transfer function, σ, is usually defined as the sigmoid function, Eqn. 13.

$$\sigma(s) = \frac{1}{1 + \exp(-s)} \quad (13)$$

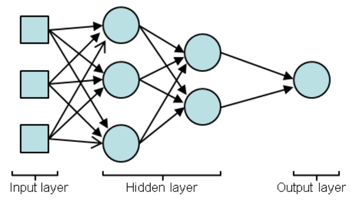

Fig. 4 Neural network structure

The weights are then trained to minimize the error between the estimated values and the exact values. In this study, the method is based on classical feedforward Neural Networks, with one hidden layer, using an efficient Levenberg-Marquardt back propagation training algorithm. The neural network is capable of handling very complex non-linear systems, and several authors report good results when used for turbomachinery applications, [6], [8] and [9] to name a few. For a detailed description of the method, see [23], [27] and [28].

3.5 Test case

The design process shown in Fig. 1(b) has been used to solve the optimization problem. The meta models were trained with 78 latin hypercube samples as the initial trainingset, which corresponds to the lowest number of designs needed to fit a second order polynom. For each outer loop, the trainingset was updated with 20 new designs, selected along the virtual pareto front. Furthermore, to verify that the meta-model assisted optimizations produced reasonable results, the same optimization problem was also solved by only using the flow solver (referred to as “discrete“). The pareto fronts from the optimizations are compared in Fig. 5 and the relative errors in each outer iteration for the meta models are summarized in Tab. 2. As can be seen, the fronts are quite similar both in location and shape in spite the general higher error estimates from the NN, Kriging and 2nd poly based optimizations. In view of the predictive relative error shown in Tab. 2, the RBF model seems to have the best performance. This was also seen during the outer loop iterations in terms of pareto front conver-

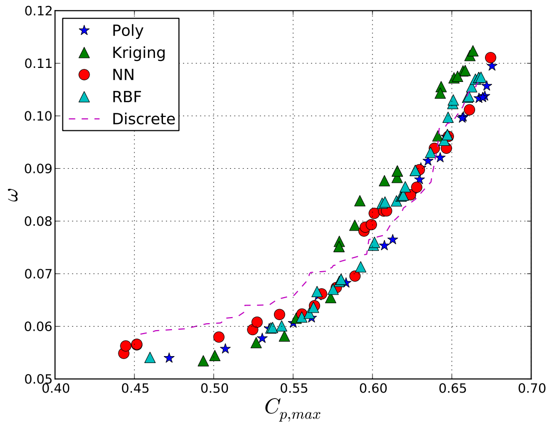

Fig. 5 Pareto front comparison based on the test case

Table 2 Summary of meta model performance based on the test case

	RBF		NN		Kriging		2nd Poly	
Outer loop	E_{max}	E_{ave}	E_{max}	E_{ave}	E_{max}	E_{ave}	E_{max}	E_{ave}
It 1	6.95%	2.55%	11.26%	5.54%	6.18%	2.72%	64.6%	53.7%
It 2	4.54%	1.45%	10.23%	4.17%	6.10%	2.82%	12.70%	5.89%
It 3	5.07%	1.23%	8.27%	2.28%	5.81%	1.02%	8.77%	2.27%
It 4	3.40%	0.71%	8.90%	3.66%	8.50%	1.21%	2.59%	1.11%
It 5	3.33%	0.59%	7.49%	2.27%	14.45%	2.23%	4.87%	1.33%

gence. The location and shape of the RBF based pareto front was converged after only three iterations while the use of the 2nd poly method to construct the meta model required five iterations.

4 Rotor re-design

The re-design of the first stage rotor of Blenda is presented in this section. The original rotor data is summarized in Tab. 3 taken from [16]. The design of Blenda is described in detail in [2]. The objective of the original rotor was to have high efficiency at the design rotational speed. The optimization was mainly driven by a 3D flow solver with a high degree of freedom in terms of design variables. The main goal with the re-design of the first stage rotor of Blenda is to verify that the new design process works in a reliable and efficient way for an industry relevant case. Furthermore, the design variables are limited compared to the original design so that the produced blades are of a more classical shape.

Table 3 Overall performance data of the Blenda rotor

Design shaft speed	22456 rpm (95.6% of max)
Tip diameter	400 mm
Tip speed	469 m/s
Hub to tip ratio	0.5
Design Mass flow	18.5 kg/s
Total-to-Total Pressure ratio	1.84

4.1 Quasi-3D results

Based on the results from the test case, the RBF was chosen to be used for the design of the first rotor of the Blenda compressor. Three radial blade profiles located at 10%, 50% and 95% span were optimized using the design process shown in Fig. 1(b). The 95.6% rotational speed is defined as the design speed while the 55% rotational speed is defined as the part speed (PS) used for maximizing the stability. As for the test case described above, the optimization problem consisted of finding the optimal blade shapes within the full parametric design space. The blade profiles were constrained to have the same mass flow capability and total-to-total pressure ratio (PrTT) as the original Blenda blade profiles. The initial trainingset was set to 78 designs and the meta model was updated for each outer loop using 20 evenly spaced designs along the virtual pareto front. After the fifth outer loop, the pareto fronts did not show any significant change, thus the optimizations were stopped. The resulting optimal solutions are compared to the Blenda blade profile performance for each radial span respectively in Fig. 6.

The change in design variables along the pareto fronts is similar for all three radial span optimizations. Furthermore, it follows the same trend as reported in [16] where only the CFD solver was used to obtain the pareto fronts. The blade shape for the best efficiency blade (ω_{opt}) is compared to the blade with the best part speed stability ($C_{p,opt}$) at 95% span in Fig. 7. As can be seen, $C_{p,opt}$ is more front loaded with a larger

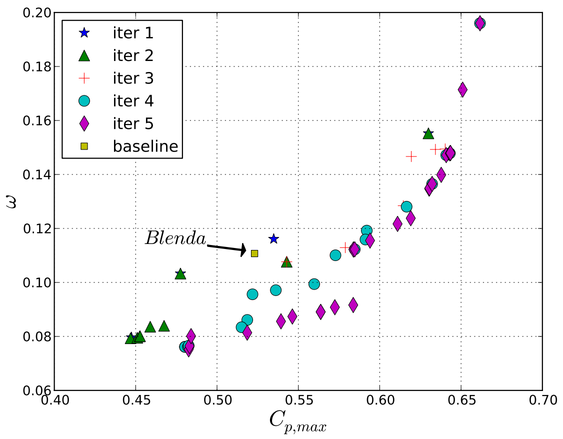

(a) 10% Span

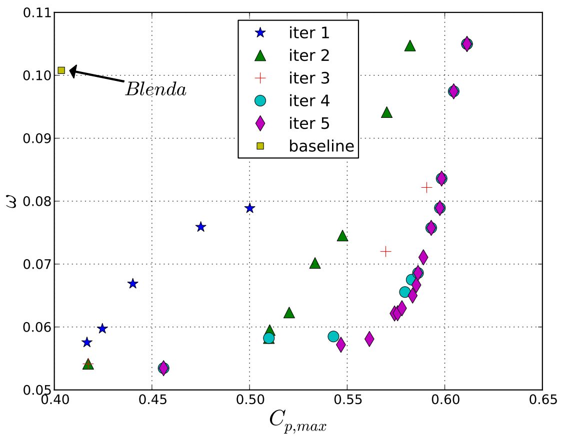

(b) 50% Span

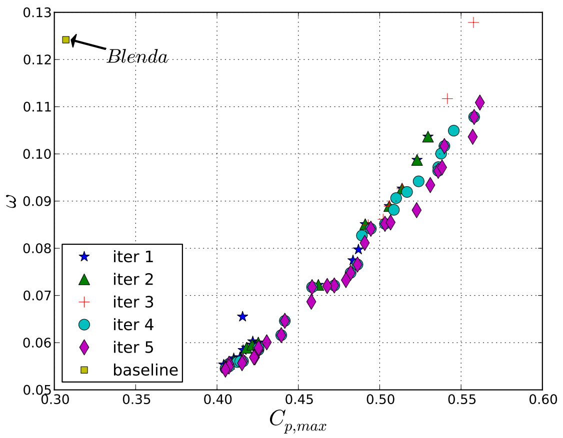

(c) 95% Span

Fig. 6 Pareto front based on the quasi-3D optimization

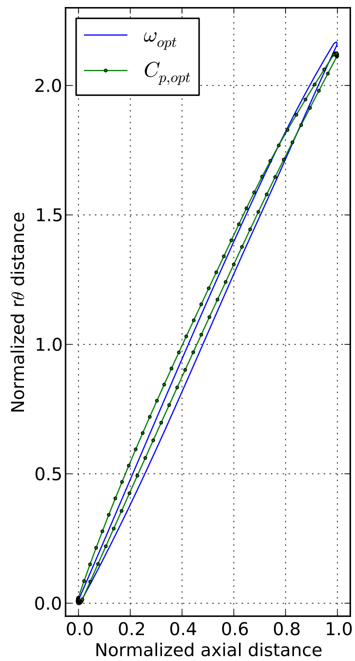

Fig. 7 Blade profile at 95% span for maximizing either of the two objectives

blade metal angle compared to ω_{opt}. Also the solidity of $C_{p,opt}$ is roughly 14% higher then ω_{opt} due to a higher blade count. The mach contours for the blades are compared in Fig. 8, where it can be seen that the lower camber of ω_{opt} leads to a lower mach number ahead of the passage shock which gives lower shock losses. However, at part speed where the incidence angle is higher, the higher camber and larger blade metal angle of $C_{p,opt}$ is needed to avoid a too high suction peak and which leads to separation as seen when comparing Fig. 9(a) to Fig. 9(b).

To obtain a baseline blade in 3D, three blade profiles were selected along the pareto front. In this study, the profile at 95% were selected to be positioned closer to the highest stability point, due to the fact that the stall problems at part speed usually originates from the poor performance of the tip sections. This profile was combined with the 10% and 50% profiles having the best efficiency. The profiles were then stacked so that their masscenter was positioned along a constant axial position. The total number of CFD based function evaluations to reach the 3D

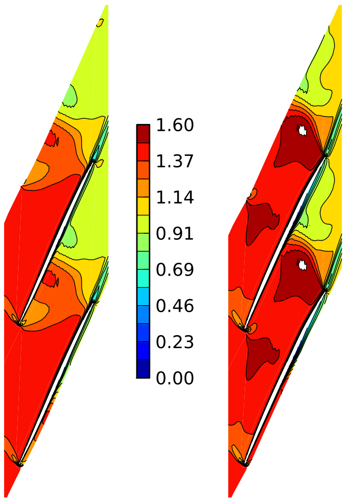

(a) ω_{opt} (b) $C_{p,opt}$

Fig. 8 Mach countour at 95% span at DP

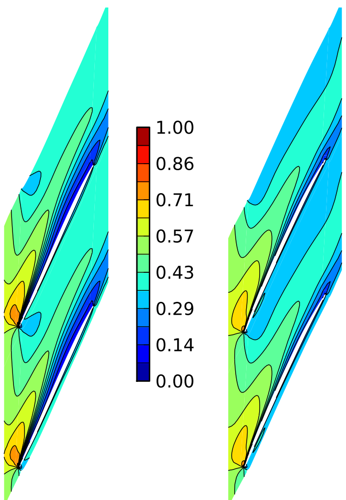

(a) ω_{opt} (b) $C_{p,opt}$

Fig. 9 Mach countour at 95% span at PS

baseline blade was 534 ($3*178$) while the pure CFD based optimization in [16] required 3000 (3*1000) evaluations. Thus by using meta model assisted optimization the total design time was reduced by 82%, which is a substantial difference.

4.2 3D optimization

The designprocess, Fig. 1(b), was once more utilized to further optimize the blade in 3D. Due to the much higher computation resources required

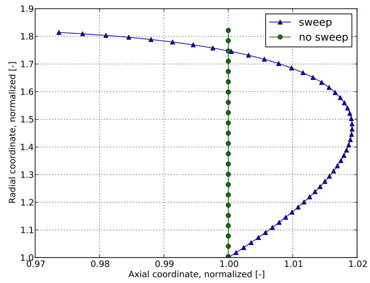

Fig. 10 Stacking line variations

to drive the optimization, the number of design variables for each radial span were reduced to include incidence, deviation and stagger angle. Also, the stacking line was varied to allow for sweep. The maximum allowed sweep within the optimization is compared to the baseline stacking line in Fig. 10. The sweep was applied by translating the blade profiles along the chordwise direction of the hub section. The meta model was initially trained using 78 latin hypercube samples. For each outer loop, 8 designs were analysed by the CFD solver and added to the updated trainingset. Again, 5 loops were required to converge the location and shape of the CFD based pareto front, seen in Fig. 11. The total number of function evaluations is thus 118. To reach a converged pareto front with a pure CFD based optimization, a minimum of around 1000 runs were required for the same pareto front resolution, thus the design time has been decreased rapidly.

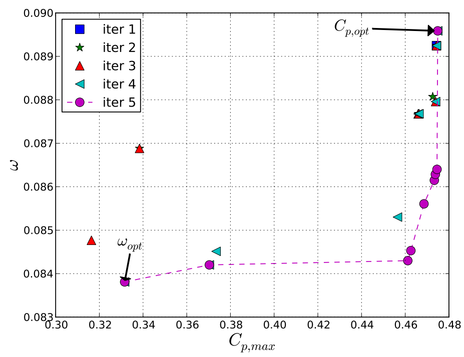

Fig. 11 Pareto from based on 3D optimization

The performance of the best efficiency design (ω_{opt}), the best stability design ($C_{p,opt}$) and the baseline design are shown in Fig. 12 and Fig. 13 together with the throttle line. As reference, the original rotor of Blenda is also included. The performance of the stacked quasi-3D optimized profiles, denoted baseline, is rather good, with a high peak efficiency and reasonably good stability at part speed relative the 3D optimized blades. However, two main problems can be seen; the operating point at design rotational speed is quite far from the peak efficiency point and the mass flow capability is off by roughly 6% compared to the goal. This issue is clearly due to the mismatch

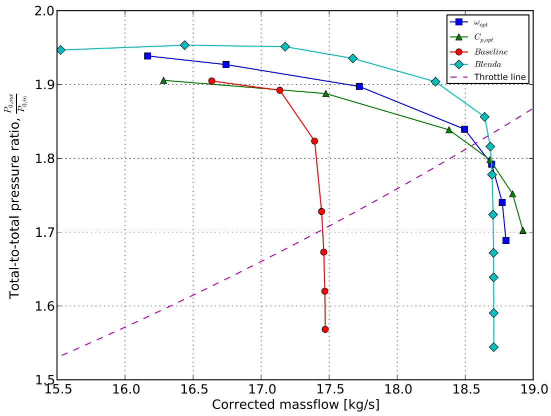

(a) Pressure ratio

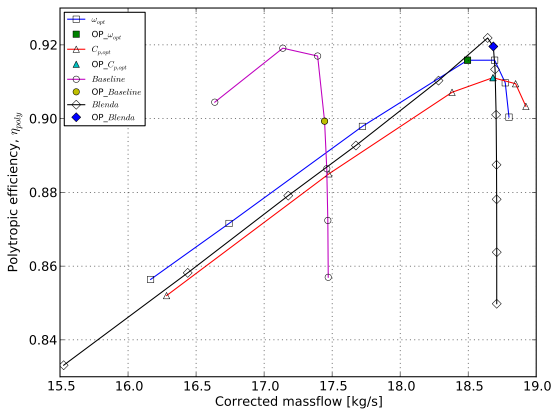

(b) Polytropic efficiency

Fig. 12 Comparison of rotor performance at 95% speed

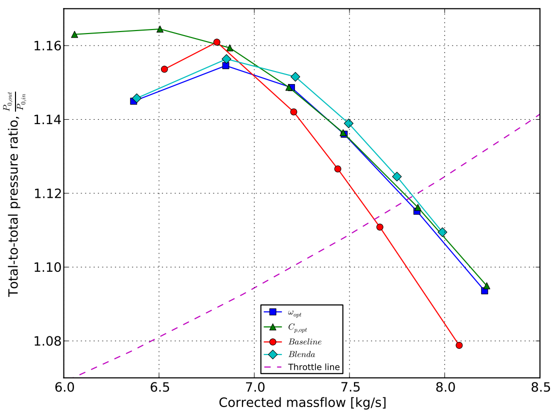

(a) Pressure ratio

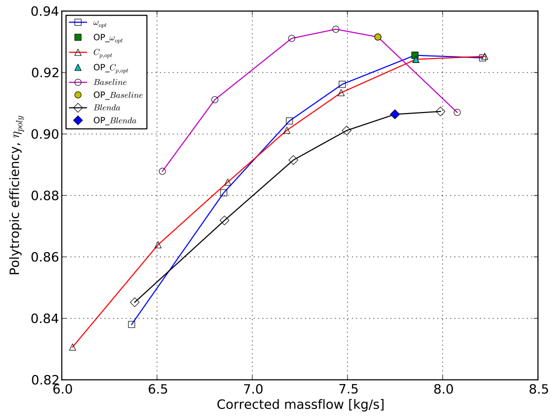

(b) Polytropic efficiency

Fig. 13 Comparison of rotor performance at 55% speed

between the quasi-3D blade to blade analysis and the full 3D analysis, also reported in [16]. During the 3D optimization, these issues vanishes since the matching of the required operating point is directly controlled. It can also be seen that the original Blenda rotor has higher peak efficiency compared to ω_{opt}, which is mainly due to the limits set in the design variables within the optimization. For instance, the optimized blades have a thicker blade root relative Blenda to reduce the blade root stress.

The blade profiles of baseline, ω_{opt} and $C_{p,opt}$ at 50% span are compared in Fig. 14. The main difference between the baseline and the 3D op-

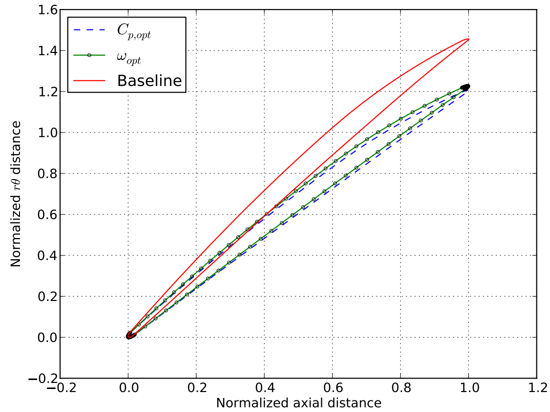

Fig. 14 Comparison of blade profiles between 3D optimized blades and baseline at 50% span

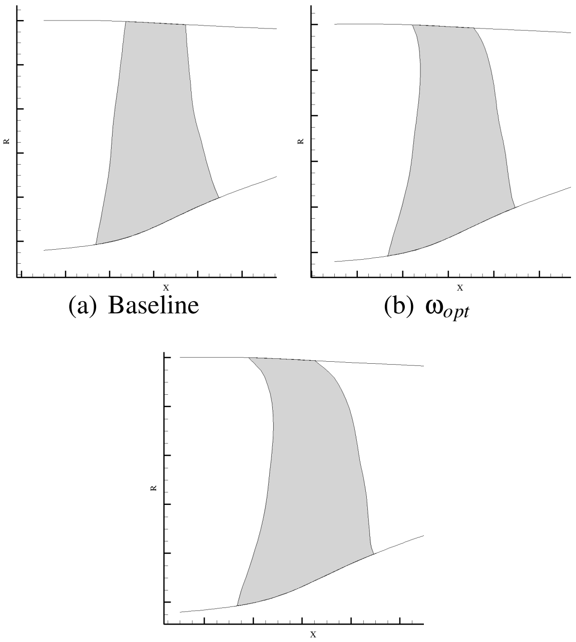

(a) Baseline (b) ω_{opt}

(c) $C_{p,opt}$

Fig. 15 Comparison of the optimized blades and the baseline in the meridional view

timized blades is the stagger angle, which has decreased to facilitate the higher massflow required at the design point. The largest difference between the two 3D optimized blades is the sweep seen in Fig. 15. At the design point, the mach number ahead of the passage shock is generally lower for ω_{opt} compared to $C_{p,opt}$ leading to lower shock losses seen in Fig. 16. This

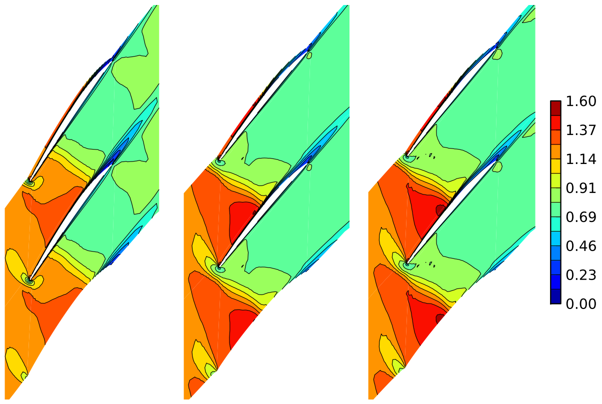

(a) Baseline (b) ω_{opt} (c) $C_{p,opt}$

Fig. 16 Mach contour at 50% span at DP

is even more pronounced for the baseline, but as mentioned above, the blade is unable to pass the required massflow rate. To find the reason why the stall margin is different for ω_{opt} and $C_{p,opt}$, the outlet effective area for each streamtube were extracted from the 3D flow results and compared at three operating points, seen in Fig. 17. Streamtubes with lower outlet effective area

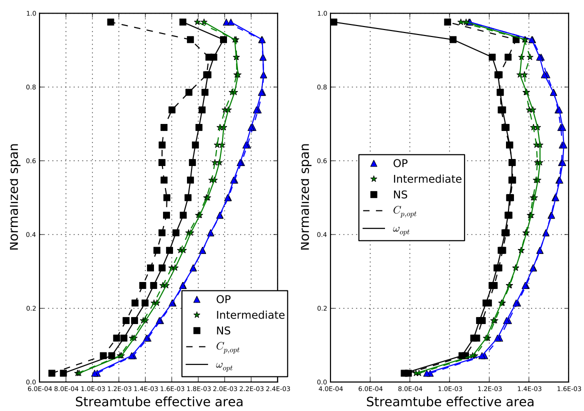

(a) DP (b) PS

Fig. 17 Outlet effective area for different throttle settings

are required to perform more diffusion, thus comparing the outlet effective area show which radial section that limits the pressure rise capability. The two designs show similar distribution at the design operating point (denoted as "OP") at both rotational speeds, see Fig. 17(a) and Fig. 17(b). However, as the rotor is throttled, the streamtubes in the vicinity of the midspan starts to deviate for $C_{p,opt}$ at the design rotational speed while the streamtubes in ω_{opt} maintains their uniformity. For the 55% rotational speed, the situation is reversed, but the region of non-uniformity appears at the tip between 80% span and the shroud. The reason to the streamtube deviation around midspan is due to a shock induced boundary layer separation at midspan seen in Fig. 18. The blades are coloured by static pressure, and the separation is visualized with an iso-surface of negative axial velocity. Downstream of the blade an outlet plane is included coloured by axial velocity. The velocity vectors are also included, extracted a few cells away from the blade wall, in order to see the fluid motion in the boundary layer. At 55% ro-

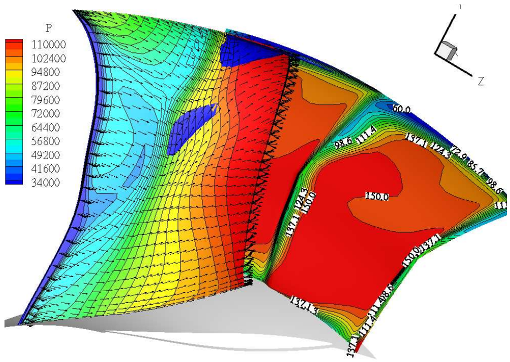

(a) ω_{opt}

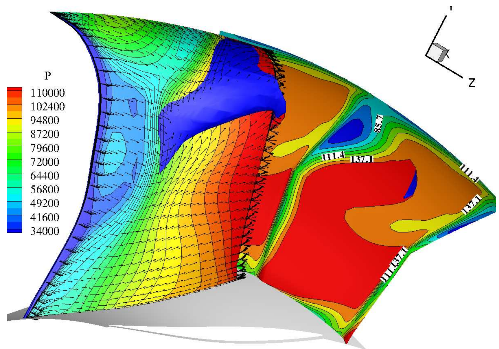

(b) $C_{p,opt}$

Fig. 18 3D flow field at near stall at 95% rotational speed

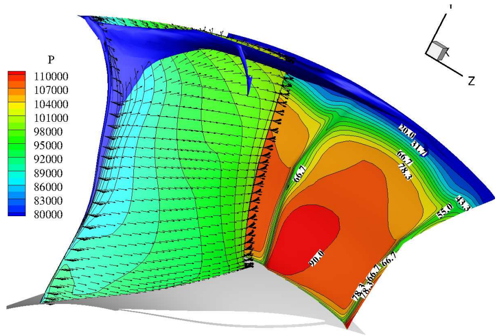

(a) ω_{opt}

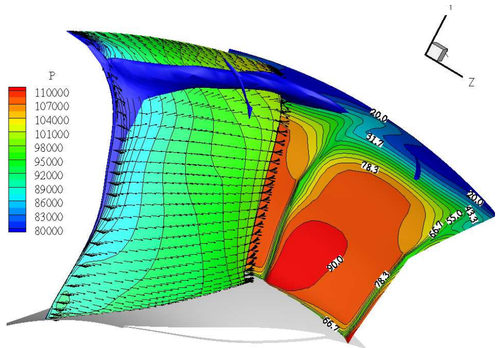

(b) $C_{p,opt}$

Fig. 19 3D flow field at near stall at 55% rotational speed

tational speed, a separated region is created just downstream of the leading edge at around 70% span, seen in Fig. 19. This low momentum fluid is pushed radially outwards due to the centrifugal force. However, due to the sweep, a high pressure region close to the shroud balance the centrifugal force. This effect is more pronounced for the higher sweep of $C_{p,opt}$. The ω_{opt} has a larger separated region and since the radial blade pressure force, is less then $C_{p,opt}$, the low momentum fluid is concentrated at the shroud, creating a large blockage which acts as a local throttle decrease. The observed trends are similar to the work in [29].

5 Conclusions

Performance comparison between several different meta models has been done for an optimization of a transonic blade profile. In this study, the radial basis functions was selected since it had the lowest predictive error of the models. The use of RBF for re-designing the first rotor of Blenda gave good results in both the optimization of blade profiles and in the 3D optimizaton. A significant decrease in computational resources have been reported compared to the case when only a flow solver has been used within the optimization. The meta model assisted optimization reduced the total design time from approximately 2 weeks to 3.5 days given that 8 designs could run in parallel on a cluster. New blades were found which increased the stability at part speed compared to the original Blenda rotor, however no blade was found which had a higher peak efficiency point relative Blenda. This is not surprising, since the design variables used in this study were limited to produce classical blade profiles. To increase the performance of the optimized blades, a higher degree of freedom is probably needed in the 3D optimization. Moreover, forward sweep has been seen to play an important role in the 3D optimization, especially when high stability is required at part speed.

References

[1] Mårtensson, H., Burman, J., and Johansson, U., 2007. "Design of the high pressure ratio transonic 1.5 stage fan demonstrator hulda". In Proceedings of ASME Turbo Expo 2007. Paper number GT2007-27793.

[2] Mårtensson, H., Langer, P., Johansson, T., Burman, J., and Lundh, C., 2009. "Design and performance of an efficient high specific power compressor". In Proceedings of ISABE 2009. Paper number ISABE-2009-1265.

[3] Köller, U., Mönig, R., Küsters, B., and Schreiber, H.-A., 2000. "Development Of Advanced Compressor Airfoils for Heavy-Duty Gas Turbines - Part I: Design and Optimization". *Journal of Turbomachinery,* ***122***(3), July, pp. 397–405.

[4] Lee, Y.-T., Luo, L., and Bein, T. W., 2001. "Direct Method for Optimization Of a Centrifugal Compressor Vaneless Diffuser". *Journal of Turbomachinery,* ***123***(1), January, pp. 73–80.

[5] Verstraete, T., 2008. "Multidisciplinary Turbomachinery Component Optimization Considering Performance, Stress, and Internal Heat Transfer". PhD Thesis, Von Karman Institute For Fluid Dynamics, June.

[6] Aulich, M., and Siller, U., 2011. "High-dimensional constrained multiobjective optimization of a fan stage". In Proceedings of ASME Turbo Expo 2011. Paper number GT2011-45618.

[7] Swoboda, A. K., Flassig, P. M., and Bestle, D., 2008. "Accelerated Industrial Blade Design B On Multi-Objective Optimization Using Surrogate model Methodology". In Proceedings of ASME Turbo Expo 2008. Paper number GT2008-50506.

[8] Schmitz, A., Aulich, M., and Nicke, E., 2011. "Novel Approach For Loss And Flow-Turning Prediction Using Optimized Surrogate Models In Two-Dimensional Compressor Design". In Proceedings of ASME Turbo Expo 2011. Paper number GT2011-45086.

[9] Huppertz, A., Flassig, P. M., Flassig, R. J., and Swoboda, M., 2007. "Knowledge-Based 2D Blade Design Using Multi-Objective Aerodynamic Optimization And A Neural Network". In Proceedings of ASME Turbo Expo 2007. Paper number GT2007-28204.

[10] Lepot, I., Mengistu, T., Hiernax, S., and Vriendt, O. D., 2011. "Highly loaded lpc blade and non axisymmetric hub profiling optimization for enhanced efficiency and stability". In Proceedings of ASME Turbo Expo 2011. Paper number GT2011-46261.

[11] Song, P., Sun, J., Wang, K., and He, Z., 2011. "Development of an optimization design method for turbomachinery by incorporating the cooperative coevolution genetic algorithm and adaptive approximate model". In Proceedings of ASME Turbo Expo 2011. Paper number GT2011-45411.

[12] A. Oyama, M-S. Liou, S. O., 2002. "Transonic axial-flow blade shape optimization using evolutionary algorithm and three-dimensional navier-stokes solver". AIAA. Paper number 2002-5642.

[13] Swoboda, M., Huppertz, A., Keskin, A., Otto, D., and Bestle, D., 2006. “Multidisciplinary compressor blading design process using automation and multi-objective optimization”. 25th Congress of International Council of the Aeronautical Sciences. Paper number ICAS2006-5.6S.

[14] Pierret, S., 2005. “Multi-objective and Multi-Disciplinary Optimization of Three-dimensional Turbomachinery Blades”. 6th World Congresses of Structural and Multidisciplinary Optimization.

[15] Peter, J., and Marcelet, M., 1981. “Comparison of surrogate models for turbomachinery design”. *WSEAS Transactions on Fluid Mechanics,* ***3***(1), October, pp. 10–17.

[16] Ellbrant, L., Eriksson, L.-E., and Mårtensson, H., 2012. “Design Of Compressor Blades Considering Efficiency And Stability Using CFD Based Optimization”. In Proceedings of ASME Turbo Expo 2012. Paper number GT2012-69272.

[17] Piegl, L., and Tiller, W., 1997. *The NURBS book*. Springer-Verlag.

[18] Burman, J., 2003. “Geometry Parameterisation and Response Surface-Based Shape Optimisation of Aero-Engine Compressors”. PhD Thesis, Luleå University Of Technology, April.

[19] J. Burman, B. R. Gebart, H. M., 2000. “Development of a blade geometry definition with implicit design variables”. AIAA. Paper number 00-67.

[20] Ellbrant, L., Eriksson, L.-E., and Mårtensson, H., 2011. “CFD Validation Of a High Speed Transonic 3.5 Stage Axial Compressor”. In Proceedings of ISABE 2011. Paper number ISABE-2011-1226.

[21] Stridh, M., and Eriksson, L.-E., 2005. “Evaluation Of Modeled Deterministic Stress Terms and Their Effects In a 3D Transonic Compressor”. In Proceedings of ISABE 2005. Paper number ISABE-2005-1100.

[22] Deb, K., Pratap, A., Agarwal, S., and Meyarivan, T., 2000. A Fast and Elitist Multi-Objective Genetic Algorithm: NSGA-II. KanGAL Report 200001, Indian Institute of Technology Kanpur, Kanpur, PIN 208 016, India.

[23] Simpson, T. W., Peplinski, J. D., Koch, P. N., and Allen, J. K., 2001. “Metamodels for computed-based engineering design: Survey and recommendations”. *Engineering with Computers,* ***17***(2), May, pp. 129–150.

[24] Giunta, A. A., and Watson, L. T., 1998. “A Comparison Of Approximation Modeling Techniques: Polynomial Versus Interpolating Models”. AIAA. Paper number AIAA-98-4758.

[25] Sacks, J., Welch, W. J., Mitchell, T. J., and Wynn, H. P., 1989. “Design and analysis of computer experiments”. *Statistical Science,* ***4***(4), May, pp. 409–435.

[26] Dyn, N., Levin, D., and Rippa, S., 1989. “Numerical procedures for surface fitting of scattered data by radial functions”. *Journal of Statistical Scientific Computing,* ***7***(2), May, pp. 639–659.

[27] Cichocki, A., and Unbehauen, R., 1994. *Neural Networks for Optimization and Signal Processing*. John Wiley and Sons.

[28] Wahde, M., 2008. *Biologically Inspired Optimization Methods*. WIT Press, Ashurst Lodge, Ashurst, Southampton, UK.

[29] Wadia, A. R., Szucs, P. N., and Crall, D. W., 1998. “Inner Workings of Aerodynamic Sweep”. *Journal of Turbomachinery,* ***120***(4), October, pp. 671–682.

5.1 Copyright Issues

The copyright statement is included in the template and must appear in your final pdf document in the position, style and font size shown below.

5.2 Copyright Statement